Electronic Supplementary Material (ESI) for Journal of Materials Chemistry C.

Supplemental Material

for

Pressure-induced Boron Clathrate with Ambient-pressure Superconductivity

Yiwei Liang, Meiling Xu*, Shuyi Lin, Xuanhao Yuan, Ziyang Qu, Jian Hao and Yinwei Li *

Laboratory of Quantum Functional Materials Design and Application, School of Physics and Electronic Engineering, Jiangsu Normal University, Xuzhou 221116, China

To whom all correspondence should be addressed.

xml@calypso.cn and yinwei_li@jsnu.edu.cn

Computational Details

The crystal structure searching is performed with CALYPSO code[1–3]. Unit cells containing 1-4 formula units were considered. In the first generation, a population of structures belonging to certain space group symmetries are randomly constructed. Starting from the second generation, 60% structures in the previous generation with the lower enthalpies are selected to produce the structures of next generation by the Particle Swarm Optimization (PSO) operators. The 40% structures in the new generation are randomly generated. A structure finger printing technique of bond characterization matrix is applied to the generated structures, so that identical structures are strictly forbidden. These procedures significantly enhance the diversity of the structures, which is crucial for structural global search efficiency. The structure search was considered converged when ~1000 successive structures were generated after a lowest energy structure was found.

The phonon spectrum and electron-phonon coupling were calculated within linear-response theory with the QUANTUM ESPRESSO code[4,5]. Ultrasoft pseudopotentials for La and B were used. The kinetic cutoff energy of 70 Ry for *R*-3*m* LaB and *P*4/*mmm* LaB_5, 80 Ry for *P*4/*mbm* LaB_4, *Cmmm* LaB_4, *Pm*-3*m* LaB_6 and *R*-3*m* LaB_8, 90 Ry for *Cmmm* LaB_6. The *q* mesh of 5×5×5 (19 *q* points), 4×4×4 (18 *q* points), 3×3×3 (8 *q* points), 5×5×5 (18 *q* points), 6×6×6 (20 *q* points), 4×4×4 (21 *q* points) and 5×5×5 (19 *q* points) for the *R*-3*m* LaB, *P*4/*mbm* LaB_4, *Cmmm* LaB_4, *P*4/*mmm* LaB_5, *Pm*-3*m* LaB_6, *Cmmm* LaB_6 and *R*-3*m* LaB_8, respectively, in the first Brillouin zone are used in the EPC calculations. Correspondingly, the *k* meshes was 20×20×20, 16×16×16, 12×12×12, 20×20×20, 24×24×24, 16×16×16 and 20×20×20 for *R*-3*m* LaB, *P*4/*mbm* LaB_4, *Cmmm* LaB_4, *P*4/*mmm* LaB_5, *Pm*-3*m* LaB_6, *Cmmm* LaB_6 and *R*-3*m* LaB_8, respectively.

Table SI. The optimized structural parameters of LaB, *Cmmm* LaB_4, LaB_5, *Cmmm* LaB_6 and LaB_8 compounds.

Phases	**Pressure (GPa)**	***a*, *b*, *c* (Å, deg)**	**Atomic position**		
R-3*m* LaB	0	*a*=*b*=*c*=8.398	La1 (2c) (0.91906	0.91906	0.91906)
		α=*γ*=*β*=23.193	B1 (2c) (0.66667	0.66667	0.66667)
Cmmm LaB_4	90	*a*=*b*=8.06570	La1 (2) (-0.31475	-0.68525	-0.50000)
		c=3.85730	La3 (2) (-0.25340	-0.25340	-0.50000)

		α=β=90.0000	B1 (4) (-0.36493	-0.94222	0.00000)
		γ=140.8757	B5 (4) (-0.35576	-0.13386	0.00000)
			B9 (4) (-0.85727	-0.14273	-0.28772)
			B13 (2) (-0.44090	-0.55910	-0.00000)
			B15 (2) (-0.05288	-0.94712	0.00000)
		a=b=3.976	La1 (1b) (0.00000	0.00000	0.50000)
*P*4/*mmm* LaB_5	80	c=2.829	B1 (1d) (0.50000	0.50000	0.50000)
		α=γ=β=90.000	B2 (4n) (0.20473	0.50000	-0.00000)
			La1 (2) (0.79536	-0.20464	-0.00000)
		a=b=5.288	B1 (4) (0.69112	-0.69112	0.79316)
		c=3.827	B2 (2) (0.88158	-0.88158	0.50000)
Cmmm LaB_6	75	α=γ=90.000	B5 (2) (0.59418	-0.40582	0.50000)
		β=77.173	B6 (4) (0.56902	-0.88300	0.50000)
			La1 (1a) (0.00000	0.00000	0.00000)
R-3*m* LaB_8	0	a=b=c=4.330	B1 (2c) (-0.70167	-0.70167	-0.70167)
		α=γ=β=77.834	B3 (6h) (-0.86527	-0.41570	-0.41570)

Table SII. The optimized structural parameters of LaB, *Cmmm* LaB_4, LaB_5, *Cmmm* LaB_6 and LaB_8 compounds.

Phases	C_{11}	C_{22}	C_{33}	C_{44}	C_{55}	C_{66}	C_{12}	C_{13}	C_{23}	B	G	H_{vc}	H_{vt}
***R*-3*m* LaB**	169	169	69	2	2	77	15	12	12	54	41	10	9
***P*4/*mbm* LaB_4**	396	396	409	144	144	148	60	51	51	170	156	32	30
***Cmmm* LaB_4**	395	340	404	147	136	176	42	45	93	166	156	32	30
***P*4/*mmm* LaB_5**	565	565	329	56	56	233	58	49	49	197	156	26	25
***Pm*-3*m* LaB_6**	476	476	476	100	100	100	23	23	23	174	150	29	27
***Cmmm* LaB_6**	439	436	447	124	45	147	75	16	70	176	125	20	19
***R*-3*m* LaB_8**	327	327	544	239	239	104	119	124	124	214	172	28	27

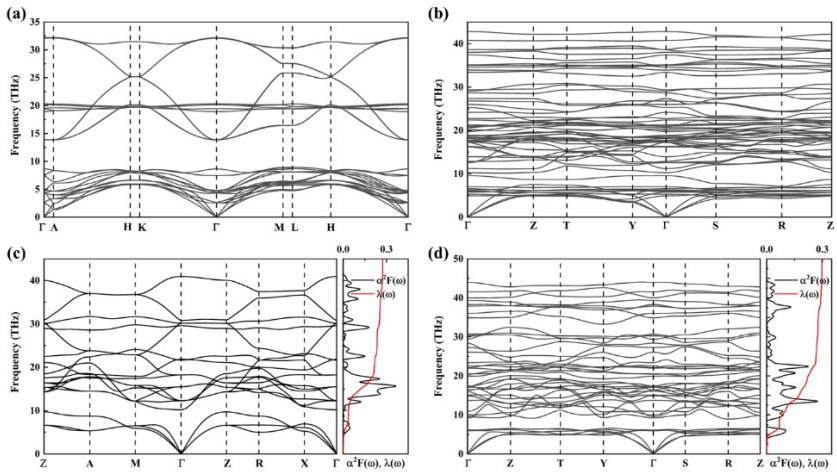

Fig. S1. The phonon dispersion relations of (a) *R*-3*m* LaB at 100 GPa, (b) *Cmmm* LaB_4 at 90 GPa. The phonon dispersion relations, Eliashberg function $\alpha^2F(\omega)$ and integrated electron-phonon coupling (EPC) strength $\lambda(\omega)$ of (c) *P*4/*mmm* LaB_5 at 80 GPa, (d) *Cmmm* LaB_6 at 75 GPa.

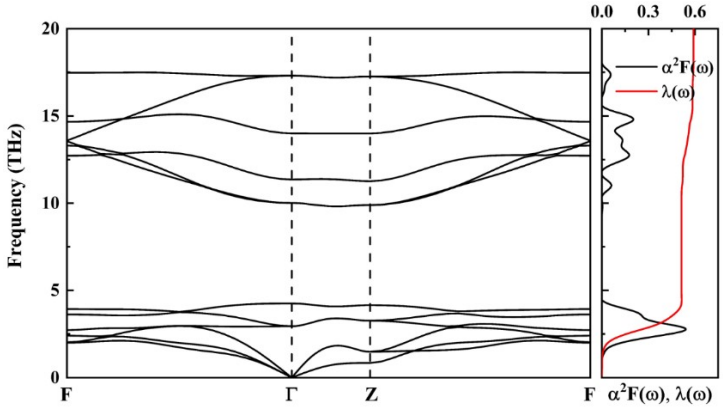

Fig. S2. The phonon dispersion relations, Eliashberg function $\alpha^2F(\omega)$ and integrated electron-phonon coupling (EPC) strength $\lambda(\omega)$ of LaB at 0 GPa.

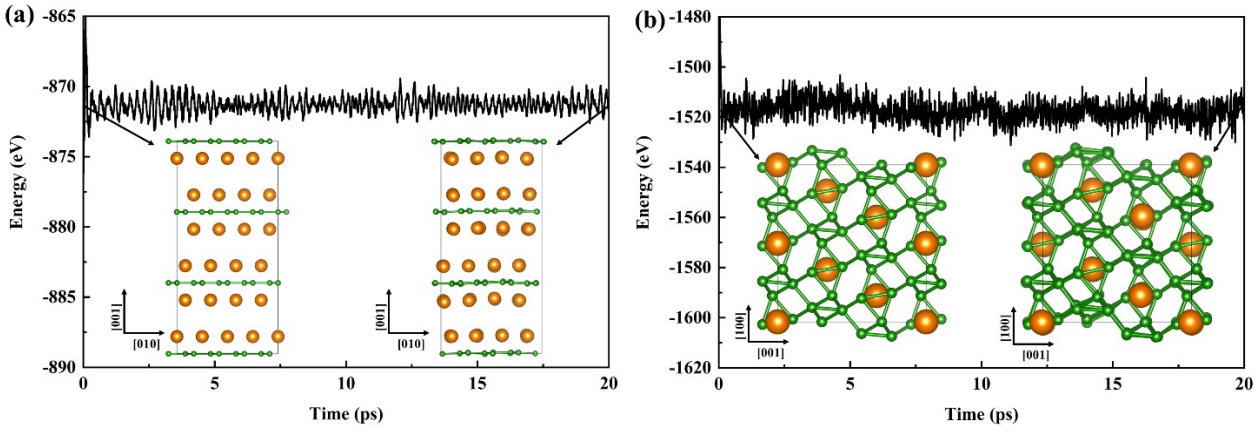

Fig. S3. Energy fluctuations during AIMD simulations up to 20 ps for (a) *R*-3*m* LaB and (b) *R*-3*m* LaB_8 at 0 GPa with 300 K.

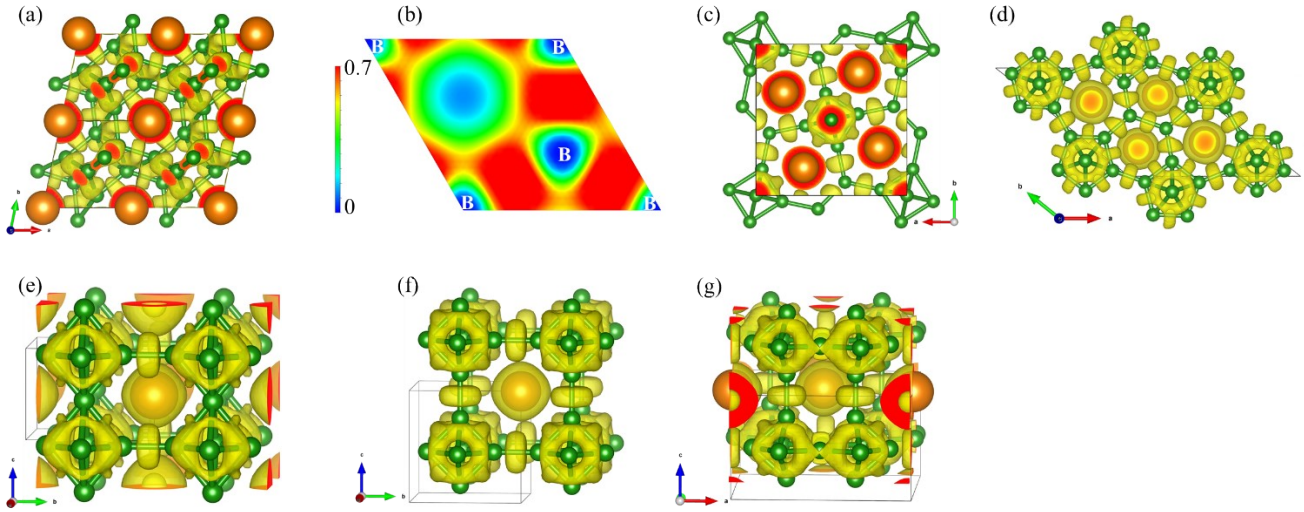

Fig. S4. Three-dimensional electron localization function (ELF) for (a) *R*-3*m* LaB_8 (c) *P*4/*mbm* LaB_4, (d) *Cmmm* LaB_4, (e) *P*4/*mmm* LaB_5, (f) *Pm*-3*m* LaB_6, (g) *Cmmm* LaB_6 and two-dimensional ELF of (b) *R*-3*m* LaB.

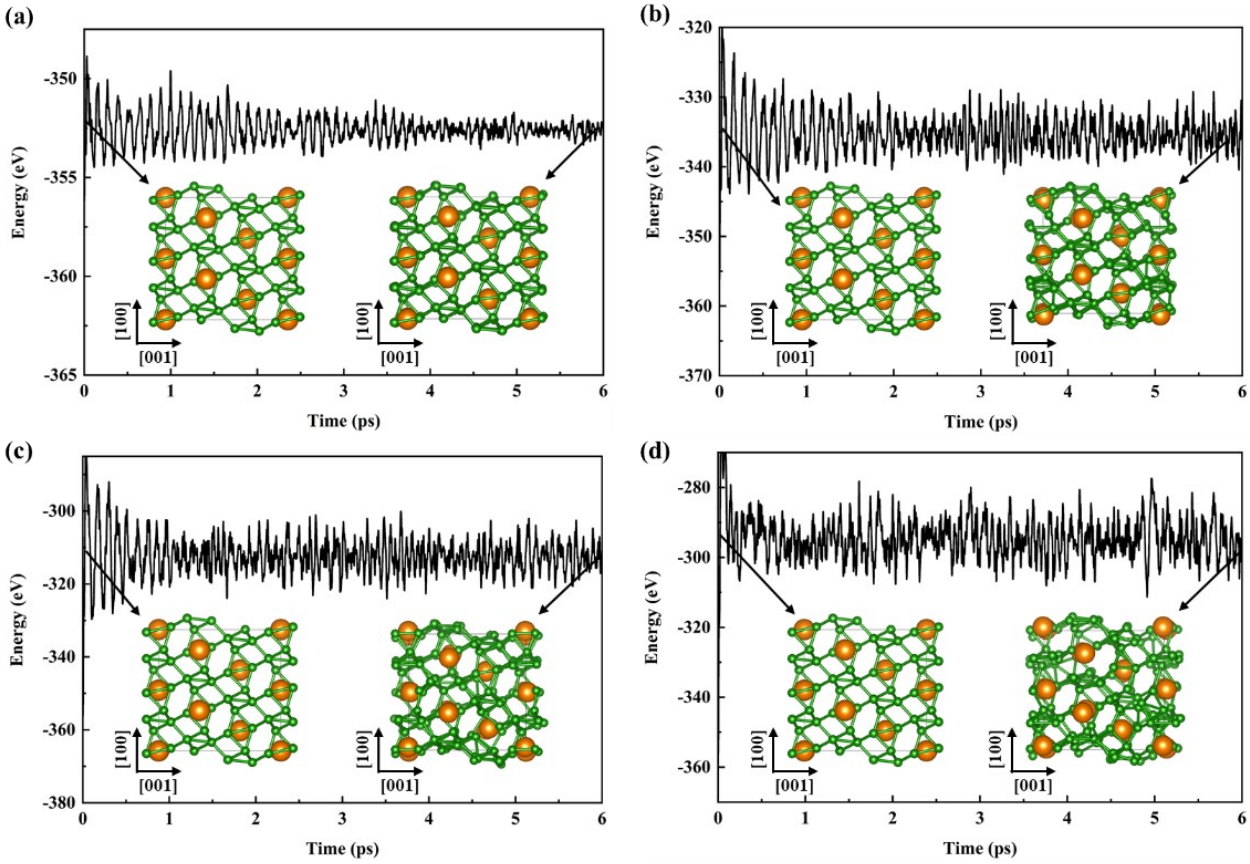

Fig. S5 Evolution of relative energies during MD simulations of LaB_8 at 70 GPa with (a) 300 K, (b) 1500 K, (c) 3000 K and (d) 4000 K. The insets are snapshots of structures at the first state and final state.

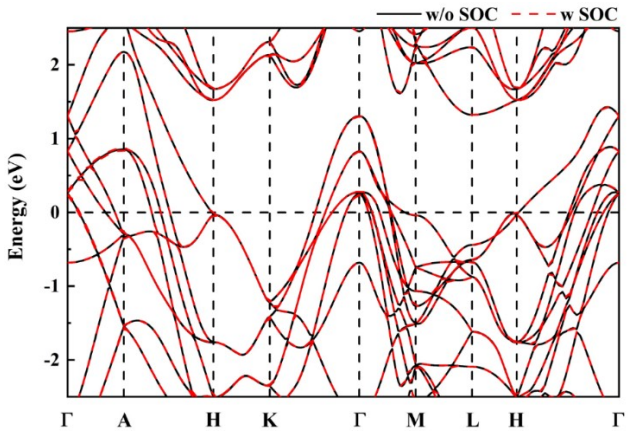

Fig. S6 Band structures of LaB_8 with and without spin-orbit effect.

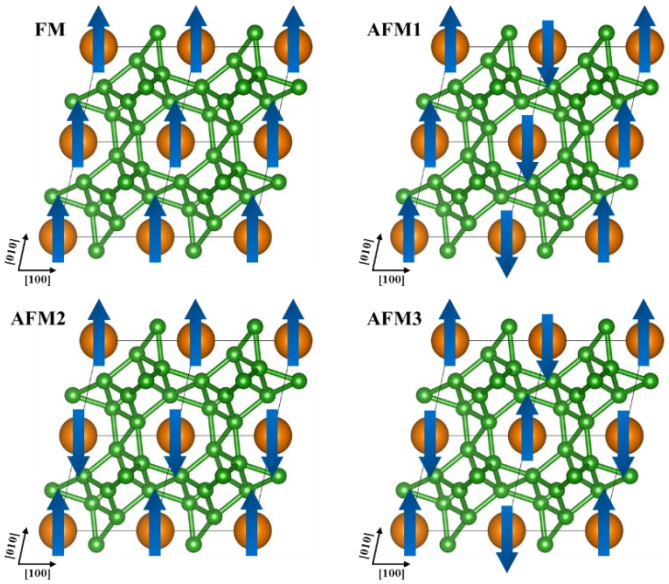

Fig. S7 Four possible magnetic configurations of LaB_8. Large and small spheres represent La and B atoms, respectively. The blue arrows represent the spin directions of La atoms. Results suggest that LaB_8 is nonmagnetic because the magnetic moment of each La atom is zero in considered magnetic phases.

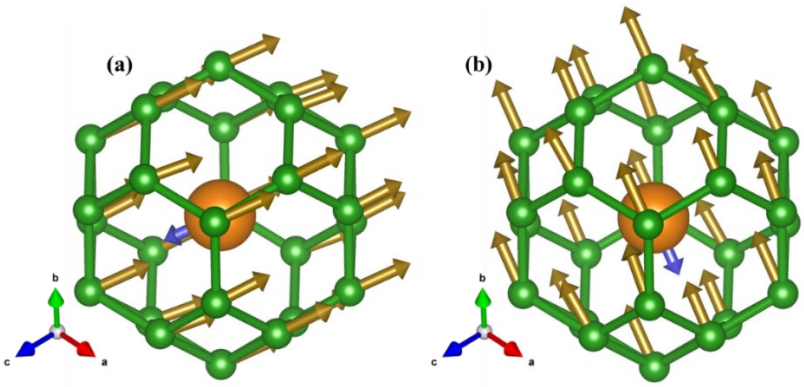

Fig. S8. Schematic illustrations of the atomic displacements of the Raman active E_u modes at the Γ point in *R*-3*m* LaB_8.

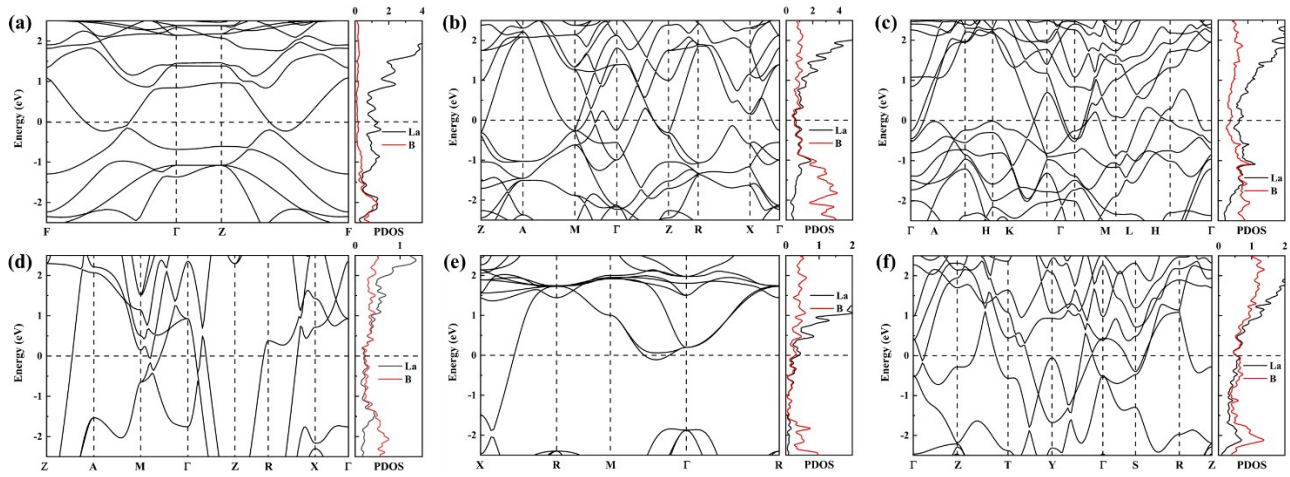

Fig. S9. Band structures and projected density of states (PDOS, in unit of states/eV/f.u.) of (a) *R*-3*m* LaB at 0 GPa, (b) *P*4/*mbm* LaB_4 at 0 GPa, (c) *Cmmm* LaB_4 at 90 GPa, (d) *P*4/*mmm* LaB_5 at 80 GPa, (e) *Pm*-3*m* LaB_6 at 0 GPa and (f) *Cmmm* LaB_6 at 75 GPa.

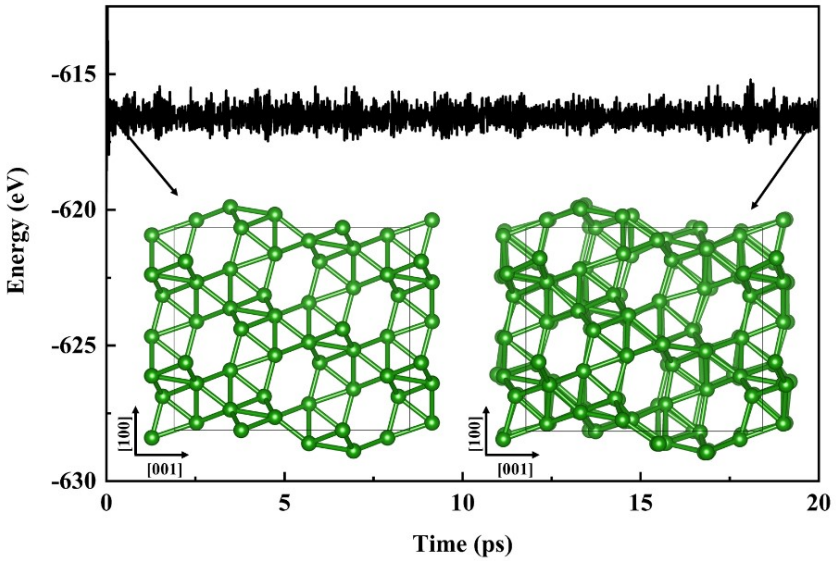

Fig. S10. Energy fluctuations during AIMD simulations up to 20 ps for the pure B_{26} cage structure at 0 GPa with 300 K.

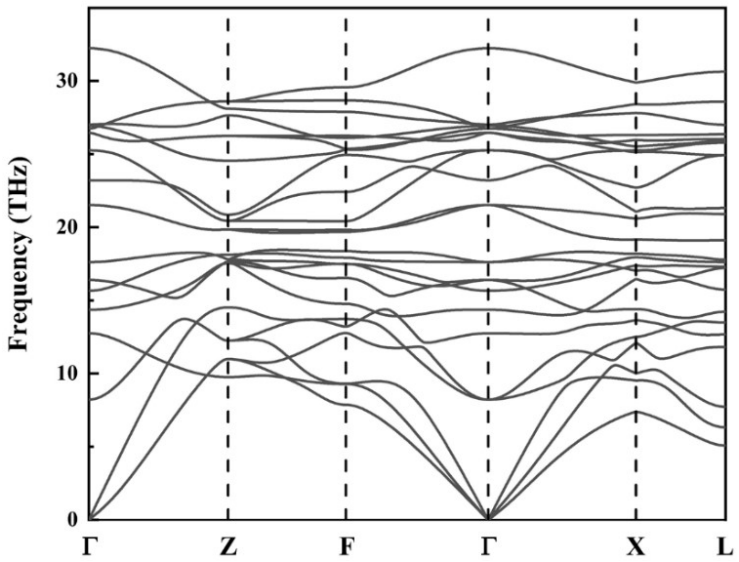

Fig. S11. Phonon dispersion relations for pure B_{26} cage at 0 GPa, which is calculated by temperature dependent effective potential method[6,7] at 300 K.

References

1 Y. Wang, J. Lv, L. Zhu and Y. Ma, *Comput. Phys. Commun.*, 2012, **183**, 2063–2070.

2 Y. Wang, J. Lv, L. Zhu and Y. Ma, *Phys. Rev. B*, 2010, **82**, 094116.

3 B. Gao, P. Gao, S. Lu, J. Lv, Y. Wang and Y. Ma, *Sci. Bull.*, 2019, **64**, 301–309.

4 S. Baroni, S. de Gironcoli, A. Dal Corso and P. Giannozzi, *Rev. Mod. Phys.*, 2001, **73**, 515–562.

5 P. Giannozzi, S. Baroni, N. Bonini, M. Calandra, R. Car, C. Cavazzoni, D. Ceresoli, G. L. Chiarotti, M. Cococcioni, I. Dabo, A. Dal Corso, S. de Gironcoli, S. Fabris, G. Fratesi, R. Gebauer, U. Gerstmann, C. Gougoussis, A. Kokalj, M. Lazzeri, L. Martin-Samos, N. Marzari, F. Mauri, R. Mazzarello, S. Paolini, A. Pasquarello, L. Paulatto, C. Sbraccia, S. Scandolo, G. Sclauzero, A. P. Seitsonen, A. Smogunov, P. Umari and R. M. Wentzcovitch, *J. Phys. Condens. Matter*, 2009, **21**, 395502.

6 O. Hellman, I. A. Abrikosov and S. I. Simak, *Phys. Rev. B*, 2011, **84**, 180301.

7 O. Hellman and I. A. Abrikosov, *Phys. Rev. B*, 2013, **88**, 144301.